electronics

MDPI

Article

Simple Modeling and Analysis of Total Ionizing Dose Effects on Radio-Frequency Low-Noise Amplifiers

Taeyeong Kim [1], Gyungtae Ryu [2], Jongho Lee [1], Moon-Kyu Cho [3], Daniel M. Fleetwood [4], John. D. Cressler [5] and Ickhyun Song [6,*]

1 Department of Semiconductor Engineering, Hanyang University, Seoul 04763, Republic of Korea; kd97050@hanyang.ac.kr (T.K.); jhlee9623@hanyang.ac.kr (J.L.)
2 Division of Nanoscale Semiconductor Engineering, Hanyang University, Seoul 04763, Republic of Korea; daeyeon36@hanyang.ac.kr
3 Department of Computer Engineering, Korea National University of Transportation, Chungju-si 27469, Republic of Korea; moonkyu.cho@ut.ac.kr
4 Department of Electrical and Computer Engineering, Vanderbilt University, Nashville, TN 37235, USA; dan.fleetwood@vanderbilt.edu
5 Department of Electrical and Computer Engineering, Georgia Institute of Technology, Atlanta, GA 30332, USA; cressler@ece.gatech.edu
6 Department of Electronic Engineering, Hanyang University, Seoul 04763, Republic of Korea
* Correspondence: isong@hanyang.ac.kr

Abstract: In this study, the degradation characteristics of radio frequency (RF)-low-noise amplifiers (LNA) due to a total ionizing dose (TID) is investigated. As a device-under-test (DUT), sample LNAs were prepared using silicon–germanium (SiGe) heterojunction bipolar transistors (HBTs) as core elements. The LNA was based on a cascode stage with emitter degeneration for narrowband applications. By using a simplified small-signal model of a SiGe HBT, design equations such as gain, impedance matching, and noise figure (NF) were derived for analyzing TID-induced degradations in the circuit-level performance. To study radiation effects in circuits, the SiGe-RF-LNAs fabricated in a commercial 350 nm SiGe technology were exposed to 10-keV X-rays to a total ionizing dose of up to 3 Mrad(SiO_2). The TID-induced performance changes of the LNA were modeled by applying degradation to device parameters. In the modeling process, new parameter values after irradiation were estimated based on information in the literature, without direct measurements of SiGe HBTs used in the LNA chip. As a result, the relative contributions of parameters on the circuit metrics were compared, identifying dominant parameters for degradation modeling. For the TID effects on input matching (S_{11}) and NF, the base resistance (R_B) and the base-to-emitter capacitance (C_π) of the input transistor were mostly responsible, whereas the transconductances (g_m) played a key role in the output matching (S_{22}) and gain (S_{21}). To validate the proposed approach, it has been applied to a different LNA in the literature and the modeling results predicted the TID-induced degradations within reasonable ranges.

Keywords: low-noise amplifier (LNA); radiation effect; radio frequency (RF); silicon–germanium heterojunction bipolar transistor (SiGe HBT); small-signal modeling; total ionizing dose (TID)

check for updates

Citation: Kim, T.; Ryu, G.; Lee, J.; Cho, M.-K.; Fleetwood, D.M.; Cressler, J.D.; Song, I. Simple Modeling and Analysis of Total Ionizing Dose Effects on Radio-Frequency Low-Noise Amplifiers. *Electronics* **2024**, *13*, 1445. https://doi.org/10.3390/electronics13081445

Academic Editors: Rafaella Fiorelli, Juan Núñez and Julián Oreggioni

Received: 19 February 2024
Revised: 7 April 2024
Accepted: 9 April 2024
Published: 11 April 2024

1. Introduction

Silicon–germanium heterojunction bipolar transistors (SiGe HBTs) have demonstrated promising suitability for a variety of wireless and communication applications. They exhibit good radio frequency (RF) performance parameters such as high unity-gain frequency (f_T) and maximum oscillation frequency (f_{MAX}) [1–3]. Moreover, in order to investigate their potential usage in extreme environment (e.g., space), radiation effects on SiGe-HBT devices and circuits have been studied in the literature [2–6]. It has been found that SiGe HBTs can often maintain performance up to an ionizing dose of hundreds of krad(SiO_2) or greater [3–6]. SiGe HBTs are not highly dependent on the quality of their oxide layers, unlike typical metal-oxide-semiconductor devices [2,3]. Still, SiGe HBTs undergo performance degradation due to total ionizing dose (TID), and they can show increases in leakage current and reductions in gain. The key mechanism associated with this degradation includes the generation of traps in the emitter-base (EB) spacer and oxide area of the shallow trench isolation (STI) [3–8].

One of the essential circuit blocks in RF applications is the low-noise amplifier (LNA) in a receiver. It is designed to provide impedance matching to the input port for good signal reception and sufficient gain for the subsequent stages, while minimizing noise contributions for better noise performance of the overall receiver system [9,10]. Regarding radiation effects, SiGe LNAs suffer from variations in input and output impedances, a reduction of signal gain, and an increase in noise figure (NF) [11], most of which are attributed to the degradation of active devices such as SiGe HBTs [12,13]. Previous workers have investigated TID effects on LNA performance [14–16], but few studies have addressed the relationships between device parameters and circuit performance. Moreover, in many cases full device-level characterization data are not available to circuit designers, imposing difficulties in analysis. Such an approach is helpful for predicting potential degradation and developing radiation-hardening design techniques that are well-trimmed to specific devices utilized in the circuit.

This paper is organized as follows. Section 2 explains the schematic and the analysis of the LNA, using simplified small-signal models of SiGe HBTs. Based on the equivalent circuit, TID-induced performance degradation is modeled. In Section 3, details of the experimental setup and performance variations of the sample SiGe LNA exposed to X-ray are presented. In Section 4, using device parameters of the equivalent circuit, we discuss modeling results and analyze the impact of SiGe-HBT parameters on LNA performance. For validating the proposed method, the modeling approach is applied to another example of an LNA in Section 5. Lastly, Section 6 summarizes the findings of this investigation.

2. LNA Schematic and Device Modeling

An RF LNA is the first gain stage in a receive chain and it plays a key role in (1) impedance matching between the antenna and the chip and (2) minimizing system noise performance. It must provide sufficient gain to the incoming signal for processing in the subsequent stages. In the aspect of small-signal operation, circuit performance is measured with scattering parameters (S-parameters); S_{21}, S_{11}, and S_{22} represent power gain, input matching, and output matching, respectively [17]. In addition, noise performance is defined as the noise figure (NF) with units of dB [18]. Large-signal characteristics of an LNA are important as well, but this work primarily focuses on small-signal operation, where signal gain, impedance matching, and noise performance are more relevant.

A target LNA employing SiGe HBTs was designed and optimized for achieving balanced gain, matching, and noise performance [18,19]. The schematic of the designed SiGe LNA is shown in Figure 1 [20–22]. This topology has been widely used for a variety of narrowband applications due to key advantages such as the ability to provide a real impedance with non-resistive components, low-noise characteristics, and good isolation between the input and the output terminals [20–22]. Specifically, the LNA was based on a cascode common-emitter (Q_1 and Q_2) stage as a main stage [5] and the second stage (Q_3 and Q_4) acted as a buffer for output-impedance matching. In the former, Q_1 was the input transistor that received the signal. Q_1, C_{BE}, L_E, and L_B were collectively optimized for the input-matching network and for noise impedance simultaneously. Q_2 was a cascode stage to improve gain performance and suppress Miller effects associated with the parasitic base-collector capacitance [23]. The emitter inductor L_E generated real impedance at the base terminal of Q_1 and provided negative feedback for stability. In addition, the base-to-emitter capacitance C_{BE} and $C_{\pi 1}$ in Figure 2 were tuned for both input and noise matching. The second branch was configured as an emitter-follower stage, providing decoupling between the first stage and the load. Lc_2 resonated out the parasitic capacitance at the collector of

Q_2, whereas Lc_1 was optimized for peak gain at the operation frequency. Lastly, C_1, C_2, and C_3 were tuned for DC blocking (or AC coupling) and R_{BIAS} supplied the desired current to the base terminal of Q_4.

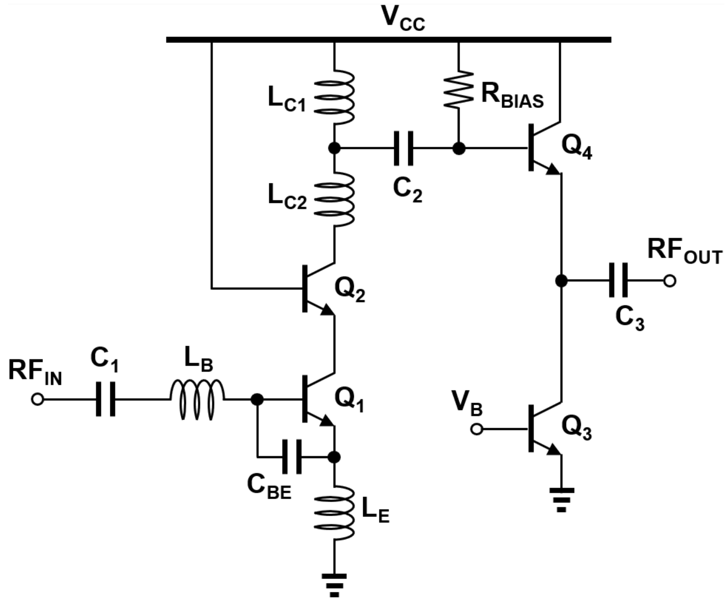

Figure 1. Circuit schematic of the designed RF SiGe LNA [20–22].

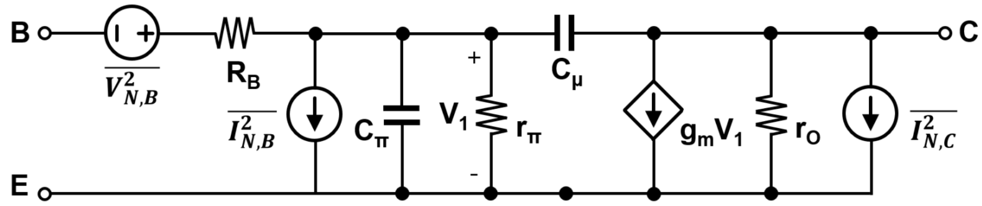

Figure 2. Small−signal model of a SiGe HBT.

For a theoretical analysis, a small-signal model of a SiGe HBT was constructed as shown in Figure 2 [24,25]. Whereas the complete small-signal-equivalent models were much more complex [26], only a few device parameters that were dominant in determining circuit performance were selected for simplicity. In this model, g_m, r_π, R_B, r_O, C_π, and C_μ represented the small-signal transconductance, the emitter-to-base resistance, the base parasitic resistance, the collector-to-emitter resistance, the base-to-emitter capacitance, and the base-to-collector capacitance, respectively. Regarding noise sources, $\overline{V_{N.B}^2}$, $\overline{I_{N.B}^2}$, and $\overline{I_{N.C}^2}$ were the thermal noise of the R_B, the shot noise associated with I_B, and the shot noise associated with I_C, respectively.

The numerical value of each parameter in the equivalent model can be obtained if full characterization results or transistor models are available, following the extract methods presented in [27]. For instance, R_B was determined from the impedance parameters (Z-parameters), whereas intrinsic capacitances C_π and C_μ were determined from the admittance parameters (Y-parameters). The transconductance (g_m) was obtained by taking the derivative of I_C with respect to V_{BE}. In this work, Equations (1)–(6) were applied to the process-design-kit models of SiGe HBTs in order to extract parameter numbers. β and ω referred to the current gain and the angular frequency, respectively.

$$g_m = \frac{\partial I_C}{\partial V_{BE}} \tag{1}$$

$$R_B = \mathrm{Re}(Z_{11} - Z_{12}) \tag{2}$$

$$r_\pi = \mathrm{Re}(Z_{12}) = \frac{\beta}{g_m} \tag{3}$$

$$r_O = \frac{\partial V_{CE}}{I_C} \tag{4}$$

$$C_\pi = \frac{\mathrm{Im}(Y_{11} + Y_{12})}{\omega} \tag{5}$$

$$C_\mu = -\frac{\mathrm{Im}(-Y_{12})}{\omega} \tag{6}$$

Once the device parameters of the SiGe HBT in the LNA were extracted, the modeling was conducted for the pre- and post-irradiation conditions [25,27]. For parameters that changed after irradiation, their values were modeled based on the information in the literature [3,4]. In this stage, circuit performance metrics such as matching, gain, and noise figure were derived as closed-form equations. For simplicity, parameters that had little or negligible contributions were omitted. For example, in the equation of the input impedance, it was mainly derived with L_B, L_E, C_{BE}, $C_{\pi1}$, and g_{m1}. Other parameters such as r_o and C_1 were assumed to be open and short, respectively. In addition, C_μ was selectively eliminated from the analysis, depending on the metrics of interest. The value of C_μ was negligible in the input impedance, but it affected the overall gain performance of the LNA. The input impedance of the LNA that incorporated the changes after irradiation is shown in Equation (7), where the real and the imaginary terms should be matched close to 50 Ω and 0 Ω for minimized reflection at the input interface. Since the dominant parameters that affected the input impedance in the post-irradiation results were the base-to-emitter capacitance ($C_{\pi1}$) and the base resistance (R_B) of the input transistor, their values were decomposed as the pre-irradiation values with "0" subscripts and delta symbols.

$$\begin{aligned} Z_{IN} &= Z_{IN,0} + \Delta Z_{IN} \\ &= \left[\frac{1}{sC_{BE}} \,||\, \left(R_{B1,0} + \Delta R_{B1} + \frac{1}{s(C_{\pi1,0}+\Delta C_{\pi1})}\right)\right] + s(L_E + L_B) \\ &\quad + \frac{(g_{m1,0}+\Delta g_{m1})L_E}{(C_{\pi1,0}+\Delta C_{\pi1})+C_{BE}+s(C_{\pi1,0}+\Delta C_{\pi1})C_{BE}(R_{B1,0}+\Delta R_{B1})} \end{aligned} \tag{7}$$

To analyze the output impedance of the LNA, the circuit was simplified as illustrated in Figure 3a. The impedance looking into the output terminal of the first branch (Z_{CAS}) that included the cascode stage was assumed to be very high (or simply an open circuit). Then, the total output impedance of the circuit (Z_{OUT}) was derived as Equation (8). In addition, r_o and C_2 were assumed to be an open and a short, respectively.

$$\begin{aligned} Z_{OUT} &= Z_{OUT,0} + \Delta Z_{OUT} \\ &= \frac{1}{r_\pi(g_{m4,0}+\Delta g_{m4})}\left[\{(R_{B4,0} + \Delta R_{B4}) + sL_{C1}\} \,||\, \frac{1}{s(C_{\mu2,0}+\Delta C_{\mu2})} + r_\pi\right] \end{aligned} \tag{8}$$

Then, since the remaining circuitry expressed real and imaginary impedances, it was further reduced to a parallel topology as shown in Figure 3b. The expressions of the components in the equivalent model were given below:

$$\begin{aligned} R_P &= R_{P,0} + \Delta R_P \\ &= \frac{(\omega_o L_{C1})^2}{\{r_\pi(g_{m4,0}+\Delta g_{m4})\}\{\omega_o^2 r_\pi(C_{\mu2,0}+\Delta C_{\mu2})L_{C1}+(R_{B4,0}+\Delta R_{B4})\}} \end{aligned} \tag{9}$$

$$L_P = L_{P,0} + \Delta L_P = \frac{L_{C1}}{r_\pi\left(g_{m4,0} + \Delta g_{m4}\right)} \tag{10}$$

$$C_P = C_{P,0} + \Delta C_P = \frac{1}{r_\pi\left(g_{m4,0} + \Delta g_{m4}\right)(C_{\mu2,0} + \Delta C_{\mu2})} \tag{11}$$

$$Z_{OUT} = Z_{OUT,0} + \Delta Z_{OUT} = R_P || sL_P || \frac{1}{sC_P} \tag{12}$$

where $\omega_0 = 2\pi f_0$ and f_0 is the operation frequency. Performance-dominant parameters in the output-impedance characteristics after TID irradiation were R_{B4} and g_{m4} of Q_4. This will be confirmed in detail by the degradation modeling in Section 4.

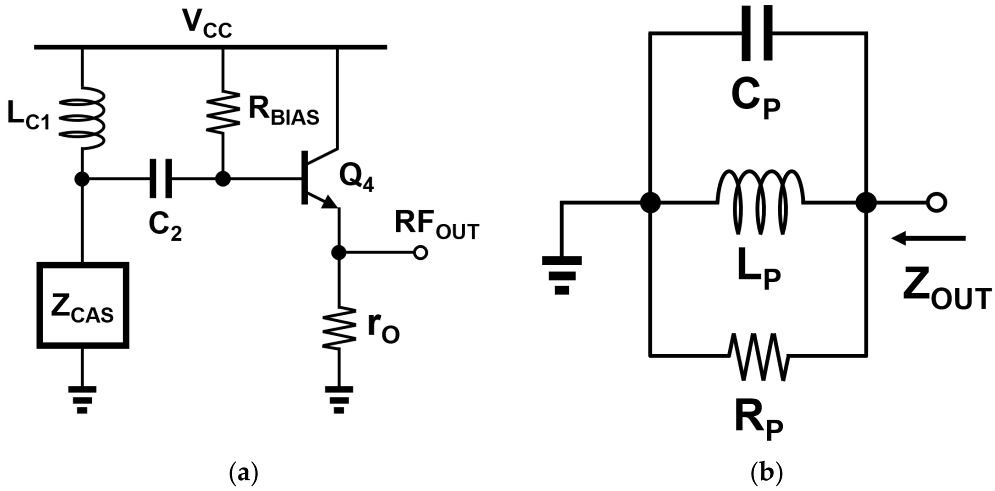

Figure 3. (**a**) Schematic to calculate the output impedance of the LNA and (**b**) the simplified RLC-equivalent model of the output impedance.

The voltage gain of the SiGe LNA was derived in Equation (13), which included dominant components of the small-signal equivalent circuit. The gain equation was composed of multiple circuit-level components (L_{C1}, L_E, and L_B) and also included transistor parameters such as g_{m1}, g_{m4}, $C_{\pi 1}$, and $C_{\pi 2}$. Similar to the input and the output-impedance equations, the parameters that most affected post-irradiation degradations were expressed with the delta terms.

$$\begin{aligned} A_{V,LNA} &= A_{V,LNA,0} + \Delta A_{V,LNA} \\ &= \frac{sL_{C1}\left[1+s^2L_E(C_{\pi1,0}+\Delta C_{\pi1})\right]\left[1+sL_E\left(g_{m1,0}+\Delta g_{m1}\right)\right]}{\left[1+s^2(L_E+L_B)(C_{BE}+C_{\pi1,0}+\Delta C_{\pi1})\right]\left(1+s\frac{C_{\pi2,0}}{g_{m2,0}}\right)}\left(1+\frac{\Delta g_{m4}}{g_{m4,0}}\right) \end{aligned} \tag{13}$$

Achieving low noise contributions from an LNA is important requirement for maintaining a high signal-to-noise ratio. In Figure 2, the thermal noise of the base resistor (R_B) and the shot noise of the base and collector currents were modeled as shown in Equations (14)–(16), which were the main sources of noise in the SiGe HBTs. In the derivation of the NF of the LNA, however, not all noise sources of the constituent transistors were included. Thus, noise contributions from the cascode- and the second-stage transistors were much smaller than those from the input transistor and were omitted. The portions of noise voltages generated from neglected parameters were estimated using the full small-signal equivalent circuits. Again, dominant parameters in the post-irradiation results were identified and corresponding delta terms were added.

$$\begin{aligned} \overline{I^2_{N.I_B}} &= \overline{I^2_{N.I_{B,0}}} + \Delta\overline{I^2_{N.I_B}} \\ &= 2q(I_{B,0} + \Delta I_B)\frac{1+sg_m L_E}{s(L_{C1}+L_{C2})}(R_{B,0} + \Delta R_B + sL_E)||(sL_E + \frac{1}{s(C_{BE}+C_{\pi,0}+\Delta C_\pi)}) \end{aligned} \tag{14}$$

$$\overline{V^2_{N.I_C}} = \overline{V^2_{N.I_{C,0}}} = 2qI_C s(L_{C1} + L_{C2})(1 - \frac{sg_m L_E}{1 + sg_m L_E}) \tag{15}$$

$$\begin{aligned} \overline{V^2_{N.R_B}} &= \overline{V^2_{N.R_{B,0}}} + \Delta\overline{V^2_{N.R_B}} \\ &= 4kT\frac{1+sg_m L_E}{s(L_{C1}+L_{C2})(R_{B,0}+\Delta R_B)}(R_{B,0} + \Delta R_B + sL_E)||(sL_E + \frac{1}{s(C_{BE}+C_{\pi,0}+\Delta C_\pi)}) \end{aligned} \tag{16}$$

$$\overline{V^2_{N.out}} = \overline{V^2_{N.out,0}} + \Delta\overline{V^2_{N.out}} = \overline{V^2_{N.R_B}} + \overline{V^2_{N.I_B}} + \overline{V^2_{N.I_C}} + 4kTR_S A^2_{V,LNA} \quad (17)$$

$$NF = NF_0 + \Delta NF = 1 + \frac{\overline{V^2_{N.out}}}{4kTR_S A^2_{V,LNA}} \quad (18)$$

Using the above equations, the performance degradation of the SiGe LNA due to TID was modeled. Results are analyzed in the next section.

3. Experimental Results

3.1. Test Setup for Performance Measurement

The designed RF SiGe LNAs in the previous section were fabricated using GlobalFoundries 350 nm SiGe BiCMOS technology, which featured a peak f_T and f_{MAX} of 23 GHz and 110 GHz, respectively [28–30]. Figure 4 shows the chip micrograph of an LNA sample. For S-parameter measurement, a network analyzer (Agilent PNA E8364B), custom-designed printed circuit boards (PCBs), and a probe station were used. Two port (input and output) measurements were calibrated using a short-open-load-through substrate (SOLT) for on-chip probing, and dc pads were wire-bonded to the board. Noise performance was characterized with a noise source (N4002A) and a PXA signal analyzer (N9030A). The supply voltage of the LNA was set to 2.5 V and the bias current of I_{BIAS1} and I_{BIAS2} were 830 μA and 600 μA, respectively. In addition, for the radiation experiment an Aracor X-ray source was used with the total dose up to 3 Mrad (SiO_2) [31–33]. An LNA sample was irradiated under unbiased conditions by disconnecting all cables from the circuit board, which could exist under deep-power-down mode or power-gating control in low-power transceiver applications [34,35]. For the case with a total of 1 Mrad(SiO_2), the dose rate was set to about 30 krad (SiO_2)/min. The time between the irradiation and the measurement was about 24 h. The pre-irradiation condition showed that the peak gain of the LNA was 12.8 dB at 6 GHz, and the spot noise figure (NF) was 3.4 dB. The input- and the output-matched frequencies were observed at 5 GHz and 5.8 GHz, respectively.

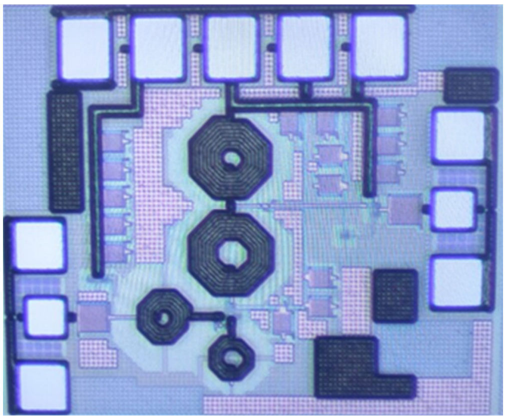

Figure 4. Microphotograph of the fabricated SiGe LNA.

3.2. Performance Degradation and Small-Signal Modeling

After the radiation experiment, branch currents did not show significant changes, implying that the collector currents of the SiGe HBTs were about the same. But the base current gradually increased (from about 8 μA to about 13 μA) as the total dose accumulated, resulting in a decrease in current gain [34]. In general, the performance of SiGe HBT LNAs was influenced by several factors, including by changes in the internal resistances and capacitances, transconductance, and/or current gain [4,35]. In this work, passive devices such as capacitors and inductors as external components were assumed to have little effect on the performance degradation [36]. The modeling of circuit performance was conducted for the pre-irradiation and the 1 Mrad cases.

Figure 5 shows the input matching (S_{11}) and the output matching (S_{22}) of the SiGe LNA for pre-irradiation and 1 Mrad cases. Comparing S_{11} and S_{22} responses, the S-parameter values increased at the matched frequencies, showing degradation in signal transfer characteristics. Regarding the locations of resonant frequencies, there were no noticeable frequency shifts between the pre- and the 1 Mrad-irradiation cases. Figure 6 shows the performance changes for power gain (S_{21}) and NF. Similar to the S_{11} and S_{22} cases, unfavorable shifts (e.g., a reduction of gain and an increase in NF) in a vertical direction were observed, but there were no noticeable horizontal shifts.

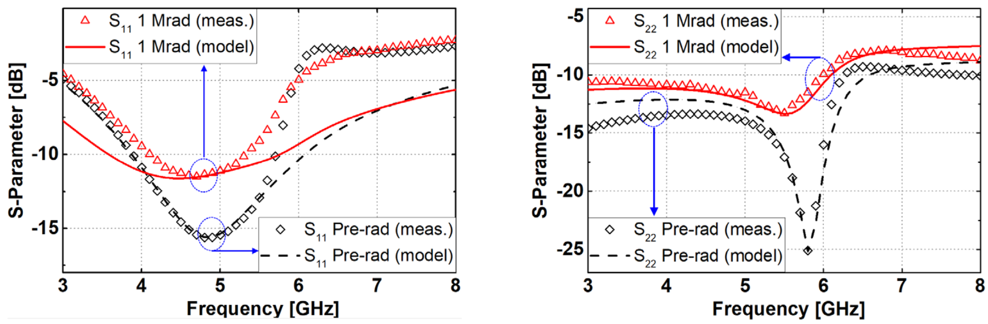

(**a**) (**b**)

Figure 5. Measured (meas.) and modeled S−parameters at pre-irradiation (pre-rad) and 1 Mrad irradiation conditions: (**a**) S_{11} (input matching) and (**b**) S_{22} (output matching) of the SiGe LNA.

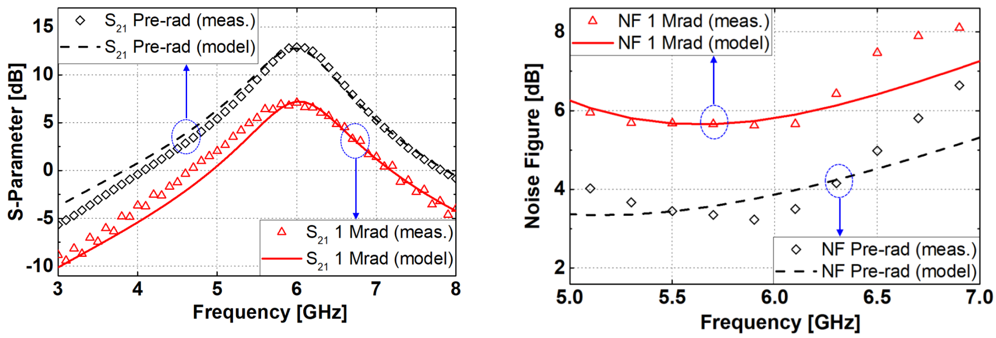

(**a**) (**b**)

Figure 6. Measured (meas.) and modeled S−parameters and noise figure (NF) at pre-irradiation (pre-rad) and 1 Mrad irradiation conditions: (**a**) S_{21} (power gain) and (**b**) NF of the SiGe LNA.

From Equations (7), (12), (13) and (18), the key LNA characteristics were modeled by assigning relevant degradation factors into device parameters, including capacitances (C_π and C_μ), g_m, and R_B. In this process, it was possible to relate them to circuit metrics, which, in turn, provided expected performance changes of similar LNAs to designers. SiGe HBTs can degrade due to irradiation traps generated in the EB spacer region, leading to an increase in the junction capacitance [4,37,38]. X-ray irradiation does not necessarily lower transconductance (g_m) [3], but slight deviations from the initial biasing point may lead to smaller g_m, degrading the gain and noise performance of a SiGe LNA [4,11,35,36]. Next, after irradiation R_B will increase due to the reduction of charge carriers, as generated traps capture a greater proportion of electrons. Moreover, dopants tend to be deactivated under the increased fluence, further raising the base resistance [18]. Therefore, it is reasonable to assume that the combined changes in device capacitances g_m and R_B will collectively affect circuit response in terms of S-parameters and NF after X-ray irradiation.

To capture and represent the TID-induced degradation characteristics, modeling based on the small-signal equivalent circuit and the design equations was performed. For example, as shown in Equation (13), the gain of the LNA was dependent on multiple parameters. With the assumption of constant values of passive components after irradiation, the changes in the gain should be modeled by assigning degradations to device-internal parameters such as the transconductances (g_m) and the base-to-emitter capacitance (C_π) of the SiGe HBTs. Similar processes were applied to the input and the output impedances and the noise of the LNA. As shown in Figures 5 and 6, the modeled results were matched around the resonant (or operation) frequencies in terms of S-parameters and NF. As frequencies move away from the center, however, some discrepancies such as magnitude and slope differences were observed, exhibiting the limitations of using simplified device models and ignored circuit parameters.

Figure 7a,b show the degradations in the input and the output-impedance matching under different total doses with reference to the pre-irradiation results, respectively. The ionizing dose caused poorer matching at the operation frequency, implying the presence of potential unwanted ripples or system instability. In addition, the gain (S_{21}) and NF characteristics exhibited overall degradations as plotted in Figure 8a,b, respectively. One thing to note was that when the TID reached the total dose of 3 Mrad(SiO_2), a slight performance recovery was observed. This was attributed to the annealing effect in the device. as the X-ray irradiation time increased, which compensated for some performance loss, and the degree of recovery over a period may vary depending on the temperature and the irradiation time [39–43]. Table 1 summaries the TID-induced changes in performance metrics under different total doses.

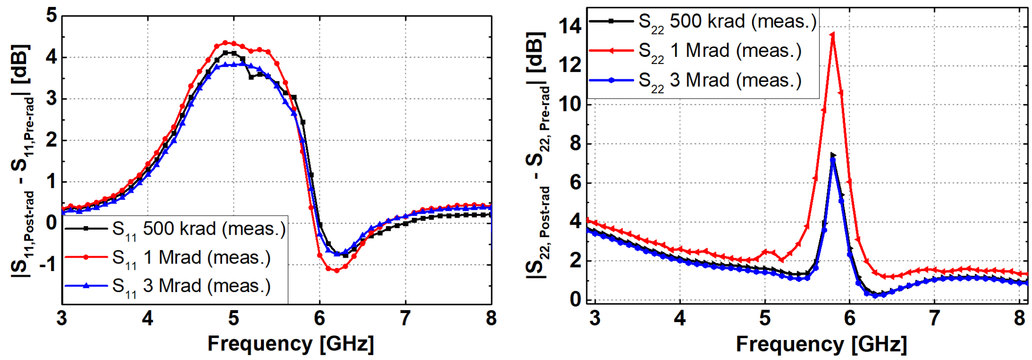

(**a**) (**b**)

Figure 7. Performance degradation with reference to the pre−irradiation condition for different total−dose cases (**a**) S_{11} (**b**) S_{22} of the SiGe LNA.

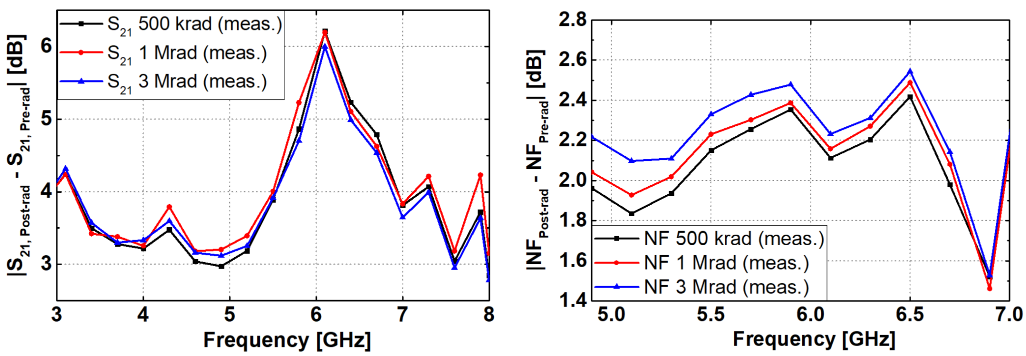

(**a**) (**b**)

Figure 8. Performance degradation with reference to the measured (meas.) pre−irradiation condition for different total−dose cases for (**a**) S_{21} (**b**) NF of the SiGe LNA.

Table 1. Degradation of LNA performance due to TID.

Total Dose	S_{11} *	S_{22} *	S_{21} +	NF *
Pre-irradiation	−15.62 dB	−23.66 dB	12.89 dB	3.45 dB
500 krad	−11.52 dB	−17.11 dB	7.34 dB	5.6 dB
1 Mrad	−11.27 dB	−11.19 dB	7.14 dB	5.66 dB
3 Mrad	−11.79 dB	−17.36 dB	7.55 dB	5.78 dB

* Numbers were negative peaks. + Numbers were positive peaks.

4. Degradation Modeling and Analysis

The degradation characteristics of SiGe HBTs due to ionizing radiation showed an increase in device resistance and capacitance, whereas g_m was reduced due to changes in the operation points, especially under the fixed current bias scheme. Based on these trends, simulations were conducted using the small-signal model of a SiGe HBT. Due to TID effects, the input and the output matching were affected by R_B, C_π, and g_m as shown in Equations (7) and (8). Changes of S_{11} (ΔS_{11}) were influenced by $\Delta C_{\pi 1}$ with a contribution of 40% and ΔR_{B1} with a contribution of 35%, as illustrated in Figure 9a. For output matching, ΔS_{22} has the largest dependency on g_{m4} at 45%, followed by $C_{\mu 2}$ (10%) (see Figure 9b). In Figure 9, other parameters contributed to ΔS_{11} and ΔS_{22}, but their portions were only about 7% and 23%, respectively.

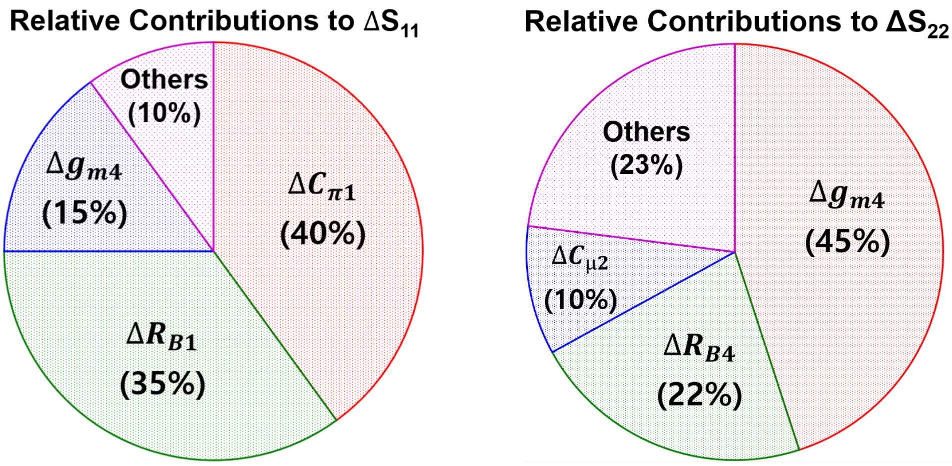

(**a**) (**b**)

Figure 9. Contribution of each parameter to performance degradation in the LNA. (**a**) Relative contributions to ΔS_{11} and (**b**) relative contributions to ΔS_{22}.

Gain changes (ΔS_{21}) were mostly affected by the decreases in transconductance (see Figure 10a). ΔS_{21} was dominated by Δg_{m4} (about 30%) and Δg_{m1} (about 20%), whereas the contributions of other capacitances such as $C_{\pi 1}$ and $C_{\mu 2}$ were much lower. Regarding noise modeling, since large portions of NF was proportional to the base resistance, it was predicted that would NF degrade as R_{B1} increased (see Figure 10b). In addition, the contribution of $C_{\pi 1}$ was ranked in the second place. Simulations using the small-signal circuit revealed that Δg_{m1} and $\Delta C_{\pi 1}$ had the most influence on NF degradation. Like the input matching and the output matching, minor parameters in gain (S_{21}) and NF (Figure 10) were responsible for only 26% and 18%, respectively. In the case of NF, the derived equation assumes perfect impedance-matching conditions. Due to TID irradiation, however, this condition might not be valid as inferred from the degradation in S_{11}. Therefore, in order to improve the modeling accuracy of NF, more parameters would be required to be included in the analysis stage.

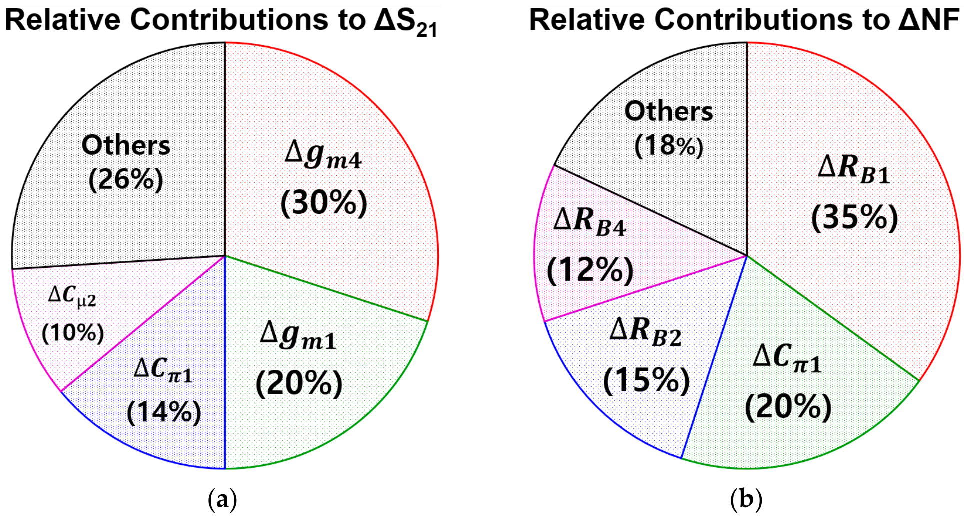

Figure 10. Contribution of each parameter to performance degradation in the LNA. (**a**) Relative contributions to ΔS_{21} and (**b**) relative contributions to ΔNF.

Table 2 summarizes the dominant parameters in the degradation of LNA performance by rank. Among many device parameters, the key contributors included $C_{\pi 1}$, R_{B1}, g_{m4}, R_{B4}, and g_{m1}. More than 90% of the change in S_{11} was attributed to degradation in the top two parameters of $C_{\pi 1}$ and R_{B1}. Regarding the change in gain (S_{21}), however, the top three parameters were responsible only for 64% of degradation. This was because the gain equation relied on multiple parameters in the equivalent circuit; a similar result was observed in the NF case. Therefore, depending on a performance metric of interest, the accuracy of the proposed approach may be different if the number of dominant parameters is limited in the modeling.

Table 2. Relative contributions of device parameters on the LNA degradation by TID.

Performance Metric	Contribution Rank #1	Contribution Rank #2	Contribution Rank #3	Portion in the Total Degradation
ΔS_{11}	$C_{\pi 1}$ (40%)	R_{B1} (35%)	g_{m1} (15%)	90%
ΔS_{22}	g_{m4} (45%)	R_{B4} (22%)	$C_{\mu 2}$ (10%)	77%
ΔS_{21}	g_{m4} (30%)	g_{m1} (20%)	$C_{\pi 1}$ (14%)	64%
ΔNF	R_{B1} (35%)	$C_{\pi 1}$ (20%)	R_{B2} (15%)	70%

Table 3 shows the variations in device parameters of SiGe HBTs before and after X-ray irradiation. In the table, it is assumed that parameters of the same-sized transistors undergo the same degree of changes, but slightly different degradation factors are allowed between transistors of different dimensions to improve modeling accuracy. The above discussion implies that proper modeling of key device parameters can predict the overall degradation characteristics due to TID effects in RF SiGe LNAs. With prior knowledge of parameter values after irradiation, the model will better estimate the performance degradation. In reality, many factors other than device parameters may affect the modeling accuracy. Dependent on the type of radiation source, the annealing effects, test configurations, and/or the materials of passive devices or PCBs, the actual modeling process should take the relevant contributions into account.

Table 3. Modeled device parameters for pre- and post-irradiation conditions.

Parameter	Unit	Pre-Irradiation	Post-Irradiation (1 Mrad)
$C_{\pi 1}$, $C_{\pi 2}$	fF	250	475
$C_{\pi 4}$	fF	240	430
$C_{\mu 1}$, $C_{\mu 2}$	fF	15	28
$C_{\mu 3}$, $C_{\mu 4}$	fF	13	25
g_{m1}, g_{m2}	mS	45	38
g_{m4}	mS	17	13
R_{B1}, R_{B2}	Ω	100	120
R_{B4}	Ω	90	110

5. Application to Another LNA Example

In order to further validate the proposed method of TID modeling in RF LNAs, the same approach was applied to an example circuit in the literature [4]. The DUT was a narrowband LNA employing a single SiGe-HBT stage with emitter degeneration as shown in Figure 11. The input-matching network was composed of two inductors (L_B and L_E) and the output matching was performed by L_C, C_C, and C_{out}.

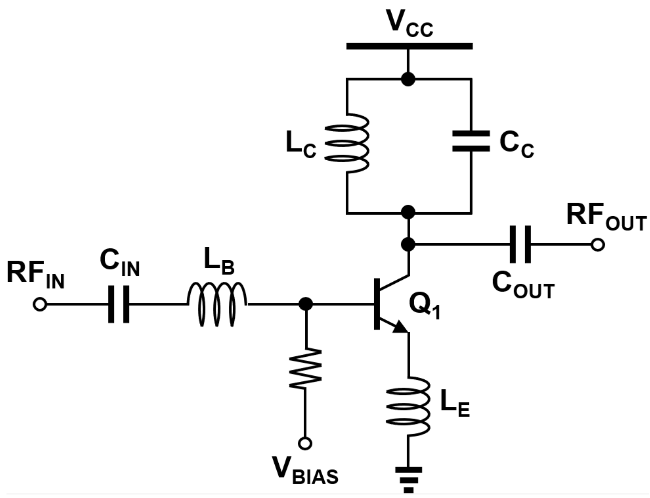

Figure 11. Circuit schematic of an RF SiGe LNA, after [4].

Each ionizing dose led to performance degradation due to changes in the device parameters such as resistance, capacitance, and transconductance of the SiGe HBT in the LNA circuits. Among various performance metrics, input matching (S_{11}) and gain (S_{21}) characteristics are modeled in this section. As the first step, the small-signal equivalent circuit was constructed with a simplified device model of the SiGe HBT. After modeling the pre-irradiation performance metrics with design equations, the range of overall degradation in each parameter was set. With the degraded parameters, the post-irradiation results were matched. The performance changes of the LNA were attributed to the changes in the base resistance, the internal parasitic capacitances, and transconductance. Their values were modeled for the fluence of 1×10^{-15} p/cm^2.

Figure 12a shows the measured and the modeled results of S_{11}, and Figure 12b shows the measured and the modeled gain (S_{21}). At the resonant frequency of 1.6 GHz, the input matching was changed from −11.6 dB to −15.8 dB, which implied that the input impedance in the pre-irradiation condition was not set at 50 Ω. After irradiation, the input matching improved. The power gain decreased by 1 dB from 18.5 dB to 17.5 dB at 1.45 GHz. Following a similar method, the post-irradiation performance was reproduced by the modeling process. Figure 13 shows the relative contributions of device parameters to the performance variations of the SiGe LNA. The top contributors in ΔS_{11} were R_B and C_π, which are the same as in the previous section; their portions were 46% and 28%, respectively. Due to the differences in the matching network and the core structure, the specific contributions of these parameters were not the same as the results in Figure 9a. Regarding the changes in S_{21}, values of g_m, R_B, and C_π were responsible for most of the degradation. The contribution of R_B to ΔS_{21} was ranked in third place. Thus, the proposed method was able to model the TID-induced degradation in RF LNAs. Depending on the topology and the technology, the impact of device parameters can be different among circuits, requiring detailed analysis based on equivalent models and design equations.

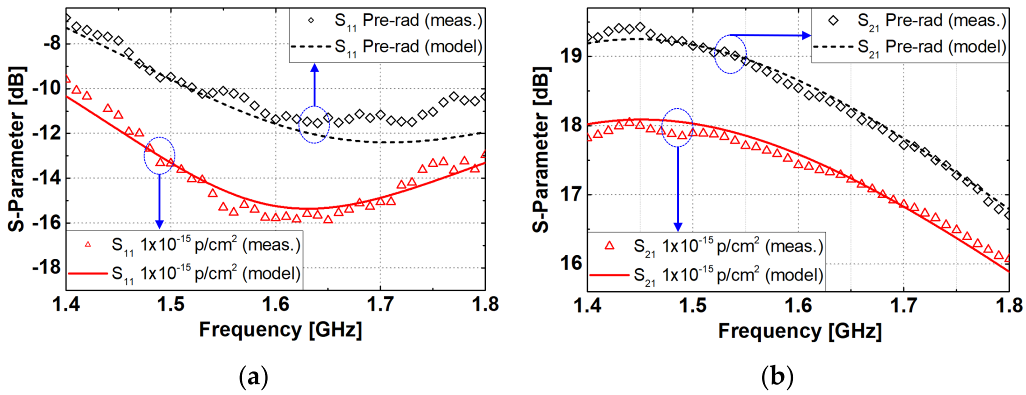

Figure 12. Measured (meas.) and modeled (**a**) S_{11} (input matching) and (**b**) S_{21} (power gain) of the example SiGe LNA described in [4].

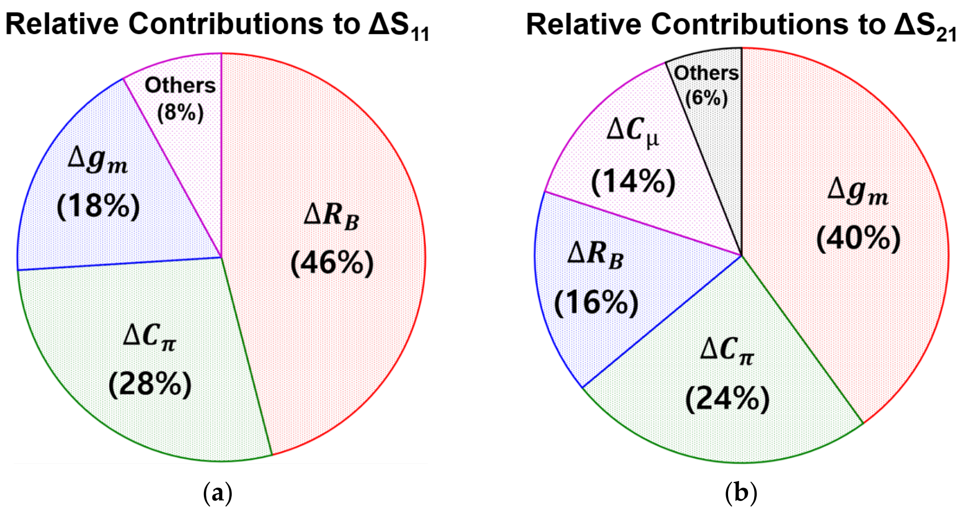

Figure 13. Contributions of each parameter to performance degradation in the LNA [4]. (**a**) Relative contributions to ΔS_{11} and (**b**) relative contributions to ΔS_{21}.

Based on the analysis of SiGe LNAs, it is worth discussing the following points about circuit design. First, the use of a buffer stage in the LNA is likely to introduce additional noticeable performance degradation. In general, a buffer provides wider matching bandwidth at the output port and less interaction between an amplifier and a load stage. In terms of S_{21}, however, changes in the transconductance of a transistor in a buffer stage led to a significant gain reduction. As shown in Figure 10a, the largest contribution to ΔS_{21} was associated with g_{m4} in the two-stage SiGe cascode LNA (Figure 1). Thus, it is recommended to minimize the use of a buffer unless there is a specific requirement. Second, inclusion of a cascode transistor lowers the impact of the changes of the base-to-collector capacitance (C_μ) in the LNA gain metric. As C_μ was not present in the gain expression Equation (13), its variations had also negligible effect on the post-irradiation results. In contrast, ΔC_μ was the fourth dominant parameter in the total gain degradation of the single-stage LNA.

By comparing Figures 10a and 13b, it was shown that the contribution of C_μ of the input transistor was much lower in the cascode LNA than in the single-ended counterpart.

In Figure 12a, it was shown that the input matching was improved by the radiation's influence, which was in the opposite direction of change in the case of the cascode LNA (Figure 5a). To allow comparison of the results, S_{11} parameters of both circuits were plotted on the Smith chart in Figure 14, showing that the changes in the real impedance were more dominant than those in the imaginary impedance. This could be attributed to the increases in R_B and C_π due to ionizing radiation, which moved the traces toward the right side as shown in Figure 14. Therefore, in terms of long-term reliability against radiation effects, the initial design of the input impedance can be targeted to slightly lower resistance than 50 Ω in order to extend the functional lifetime of the LNA under TID irradiation. From the experiments, the shifts in the center frequencies are expected to be less severe than magnitude changes. In addition, the use of a cascode stage and the elimination of a buffer will effectively minimize performance variations in LNAs.

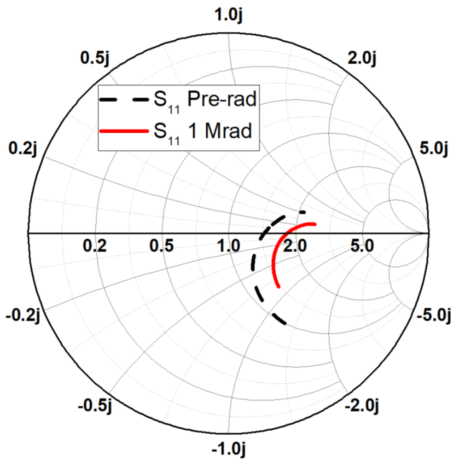

(**a**)

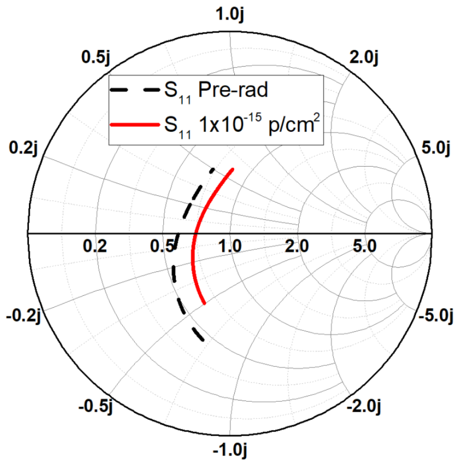

(**b**)

Figure 14. Modeled S_{11} plotted on a Smith chart; (**a**) SiGe cascode LNA (Figure 5a) and (**b**) SiGe single-stage LNA (Figure 12a) [4].

6. Summary

Degradation characteristics of an RF SiGe LNA under TID effects are investigated using a small-signal equivalent model of a SiGe HBT. Based on the design equations of the LNA, the performance changes due to 1 Mrad(SiO_2) X-ray irradiation are modeled for input matching and output matching, gain, and noise figure characteristics. It is observed that for each circuit metric, the relative contributions of the device parameters were different. Among many parameters, transconductances, base resistances, and base-to-emitter capacitances were mostly responsible for the degradation of the LNA performance. The proposed approach not only provides the relationship between device parameters and circuit metrics but also identifies the dominant parameters that are critical in modeling TID responses. In addition, the proposed method is applied to a different example LNA circuit, exhibiting the ability to reproduce radiation effects with reasonable accuracy. Therefore, the findings of this work can be utilized to effectively predict potential degradations in RF SiGe LNAs due to TID, which will be useful in the early-stage evaluation of radiation sensitivity or hardness.

Author Contributions: Conceptualization, T.K. and I.S.; methodology, T.K. and I.S.; software, J.L.; validation, T.K., M.-K.C. and I.S.; formal analysis, T.K., J.L. and I.S.; investigation, T.K. and M.-K.C.; resources, D.M.F., J.D.C. and I.S.; data curation, J.L.; writing—original draft preparation, T.K., G.R. and I.S.; writing—review and editing, M.-K.C. and I.S.; visualization, T.K.; supervision, J.D.C. and I.S.; project administration, J.D.C. and I.S.; funding acquisition, J.D.C. and I.S. All authors have read and agreed to the published version of the manuscript.

Funding: This work was supported in part by National Research Foundation of Korea (NRF) grants funded by the Korea government (MSIT) (No. NRF-2022M1A3B8076511, NRF-2022M3I7A1085472, and RS-2023-00212268) and in part by the Institute of Information and Communications Technology Planning and Evaluation (IITP) under the artificial intelligence semiconductor support program to nurture the best talent (IITP-2024-RS-2023-00253914) grant funded by the Korea government (MSIT). In addition, this research was supported in part by the "Regional Innovation Strategy (RIS)" through the National Research Foundation of Korea (NRF) funded by the Ministry of Education (MOE) (2021RIS-001). The EDA tool was supported by the IC Design Education Center (IDEC), Korea.

Data Availability Statement: Data is contained within the article.

Conflicts of Interest: The authors declare no conflicts of interest.

References

1. Kanar, T.; Rebeiz, G.M. X- and K-band SiGe HBT LNAs with 1.2- and 2.2-dB mean noise figures. *IEEE Trans. Microw. Theory Tech.* **2014**, *62*, 2381–2389. [CrossRef]
2. Song, I.; Cardoso, A.S.; Ying, H.; Cho, M.-K.; Cressler, J.D. Cryogenic characterization of RF low-noise amplifiers utilizing inverse-mode SiGe HBTs for extreme environment applications. *IEEE Trans. Device Mater. Reliab.* **2018**, *18*, 613–619. [CrossRef]
3. Cressler, J.D. Radiation Effects in SiGe Technology. *IEEE Trans. Nucl. Sci.* **2013**, *60*, 1992–2014. [CrossRef]
4. Li, Z.; Liu, S.; Ren, X.; Adekoya, M.A.; Zhang, J.; Liu, S. Experimental investigation on the degradation of SiGe LNAs under different bias conditions induced by 3 MeV proton irradiation. *Nucl. Eng. Technol.* **2022**, *54*, 661–665. [CrossRef]
5. Wei, J.; He, C.; Zhang, P.; Fu, X.; Guo, H.; Luo, T. Impact of Ge profile on TID susceptibility of SiGe HBTs. In Proceedings of the 2021 4th International Conference on Radiation Effects of Electronic Devices (ICREED), Xi'an, China, 26–29 May 2021. [CrossRef]
6. Ullan, M.; Diez, S.; Campabadal, F.; Lozano, M.; Pellegrini, G.; Knoll, D.; Heinemann, B. Gamma radiation effects on different varieties of SiGe:C HBT technologies. *IEEE Trans. Nucl. Sci.* **2007**, *54*, 989–993. [CrossRef]
7. Zhang, J.X.; Guo, Q.; Guo, H.-X.; Lu, W.; He, C.-H.; Wang, X.; Li, P.; Lin, W. Investigation of enhanced low dose rate sensitivity in SiGe HBTs by ^{60}Co γ irradiation under different biases. *Microelectron. Reliab.* **2018**, *84*, 105–111. [CrossRef]
8. Petrosyants, K.O.; Kozhukhov, M.V. Physical TCAD Model for Proton Radiation Effects in SiGe HBTs. *IEEE Trans. Nucl. Sci.* **2016**, *63*, 2016–2021. [CrossRef]
9. Lerdworatawee, J.; Namgoong, W. Wide-band CMOS cascode low-noise amplifier design based on source degeneration topology. *IEEE Trans. Circuits Syst. I Reg. Papers* **2005**, *52*, 2327–2334. [CrossRef]
10. Li, Z.; Liu, S.; Adekoya, M.A.; Ren, X.; Zhang, J.; Liu, S.; Li, L. Radiation response of SiGe low noise amplifier irradiated with different energy protons. *Microelectron. Reliab.* **2021**, *127*, 114396. [CrossRef]
11. Sarker, M.A.R.; Jung, S.; Ildefonso, A.; Khachatrian, A.; Buchner, S.P.; McMorrow, D.; Paki, P.; Cressler, J.D.; Song, I. Mitigation of single-event effects in SiGe-HBT current-mode logic circuits. *Sensors* **2020**, *20*, 2581. [CrossRef] [PubMed]
12. Zhang, J.; Guo, Q.; Guo, H.; Lu, W.; He, C.; Wang, X.; Li, P.; Liu, M. Impact of bias conditions on total ionizing dose effects of ^{60}Coγ in SiGe HBT. *IEEE Trans. Nucl. Sci.* **2016**, *63*, 1251–1258. [CrossRef]
13. Minko, F.S.; Stander, T. Effect of TID electronradiation on SiGe BiCMOS LNAs at V-band. *Microelectron. Reliab.* **2020**, *112*, 113750. [CrossRef]
14. Mossawir, B.; Linscott, I.R.; Inan, U.S.; Roeder, J.L.; Osborn, J.V.; Witczak, S.C.; King, E.E.; LaLumondiere, S.D. A TID and SEE radiation-hardened, wideband, low-noise amplifier. *IEEE Trans. Nucl. Sci.* **2006**, *53*, 3439–3448. [CrossRef]
15. Fu, X.; You, D.; Wang, X.; Wang, Y.; Mayeda, C.J.; Gao, Y.; Zhang, Y.; Sakamaki, J.; Fadila, A.A.; Li, Z.; et al. A low-power 256-element Ka-band CMOS phased-array receiver with on-chip distributed radiation sensors for small satellite constellations. *IEEE J. Solid-State Circuits* **2023**, *58*, 3380–3395. [CrossRef]
16. Kobal, E.; Siriburanon, T.; Staszewski, R.B.; Zhu, A. A compact, low-power, low-NF, millimeter-wave cascode LNA with magnetic coupling feedback in 22-nm FD-SOI CMOS for 5G applications. *IEEE Trans. Circuits Syst. II Exp. Briefs* **2023**, *70*, 1331–1335. [CrossRef]
17. Jia, X.; Niu, G. Impact of correlated RF noise on SiGe HBT noise parameters and LNA design implications. *IEEE Trans. Electron Devices* **2014**, *61*, 2324–2331. [CrossRef]
18. Weinreb, S.; Bardin, J.C.; Mani, H. Design of cryogenic SiGe low-noise amplifiers. *IEEE Trans. Microw. Theory Tech.* **2007**, *55*, 2306–2312. [CrossRef]
19. Fan, X.; Zhang, H.; Sánchez-Sinencio, E. A noise reduction and linearity improvement technique for a differential cascode LNA. *IEEE J. Solid-State Circuits* **2008**, *43*, 588–599. [CrossRef]
20. Bimana, A.; Sinha, S. Impact of SiGe HBT parameters to the performance of LNAs for highly sensitive SKA receivers. In Proceedings of the 2013 23rd International Conference Radioelektronika (RADIOELEKTRONIKA), Pardubice, Czech Republic, 16–17 April 2013. [CrossRef]
21. Shaeffer, D.K.; Lee, T.H. A 1.5-V, 1.5-GHz CMOS low noise amplifier. *IEEE J. Solid-State Circuits* **1997**, *32*, 745–759. [CrossRef]
22. Song, I.; Ryu, G.; Jung, S.H.; Cressler, J.D.; Cho, M.-K. Wideband SiGe-HBT low-noise amplifier with resistive feedback and shunt peaking. *Sensors* **2023**, *23*, 6745. [CrossRef]

23. Lee, S.; Ryum, B.R.; Kang, S.W. A new parameter extraction technique for small-signal equivalent circuit of polysilicon emitter bipolar transistors. *IEEE Trans. Electron Devices* **1994**, *41*, 233–238. [CrossRef]
24. Sarker, M.A.R.; Song, I. Design and analysis of f_T-doubler-based RF amplifiers in SiGe HBT technology. *Electronics* **2020**, *9*, 772. [CrossRef]
25. Sun, Y.; Fu, J.; Wang, Y.; Zhou, W.; Zang, W.; Liu, J. Direct analytical parameter extraction for SiGe HBTs T-topology small-signal equivalent circuit. *Superlattices Microstruct.* **2016**, *94*, 223–230. [CrossRef]
26. Lee, K.; Choi, K.; Kook, S.H.; Cho, D.H.; Park, K.W.; Kim, B. Direct parameter extraction of SiGe HBTs for the VBIC bipolar compact model. *IEEE Trans. Electron Devices* **2005**, *52*, 375–384. [CrossRef]
27. SiGe Power Amplifier Platforms. Available online: http://gf.com/wp-content/uploads/2021/12/GF21-SiGe-PA-0705.pdf (accessed on 16 February 2024).
28. Sirohi, S.; Sirohi, S.; Jain, V.; Raman, A.; Nukala, B.; Veeramani, E.; Adkisson, J.W.; Joseph, A. impact of emitter width scaling on performance and ruggedness of SiGe HBTs for PA applications. In Proceedings of the 2018 IEEE BiCMOS and Compound Semiconductor Integrated Circuits and Technology Symposium (BCICTS), San Diego, CA, USA, 15–17 October 2018. [CrossRef]
29. Song, I.; Cho, M.K.; Lourenco, N.E.; Fleetwood, Z.E.; Jung, S.; Roche, N.J.-H.; Khachatrian, A.; Buchner, S.P.; McMorrow, D.; Paki, P.; et al. The use of inverse-mode SiGe HBTs as active gain stages in low-noise amplifiers for the mitigation of single-event transients. *IEEE Trans. Nucl. Sci.* **2017**, *64*, 359–366. [CrossRef]
30. Gorchichko, M.; Cao, Y.; Zhang, E.X.; Yan, D.; Gong, H.; Zhao, S.E.; Wang, P.; Jiang, R.; Liang, C.; Fleetwood, D.M.; et al. Total-ionizing-dose effects and low-frequency noise in 30-nm gate-length bulk and SOI FinFETs With SiO_2/HfO_2 gate dielectrics. *IEEE Trans. Nucl. Sci.* **2020**, *67*, 245–252. [CrossRef]
31. Lambert, D.; Gaillardin, M.; Raine, M.; Paillet, P.; Duhamel, O.; Marcandella, C.; Martinez, M.; Rostand, N.; Lagutère, T.; Aubert, D.; et al. TID effects induced by ARACOR, ^{60}Co, and ORIATRON photon sources in MOS devices: Impact of geometry and materials. *IEEE Trans. Nucl. Sci.* **2021**, *68*, 991–1001. [CrossRef]
32. Gaillardin, M.; Lambert, D.; Aubert, D.; Raine, M.; Marcandella, C.; Assaillit, G.; Auriel, G.; Martinez, M.; Duhamel, O.; Ribière, M.; et al. Investigations on spectral photon radiation sources to perform TID experiments in micro- and nano-electronic devices. *IEEE Trans. Nucl. Sci.* **2021**, *68*, 928–936. [CrossRef]
33. Ullán, M.; Díez, S.; Campabadal, F.; Lozano, M.; Pellegrini, G.; Knoll, D.; Heinemann, B. Radiation hardness evaluation of SiGe HBT technologies for the front-end electronics of the ATLAS upgrade. *Nucl. Instrum. Methods Phys. Res. A* **2007**, *579*, 828–832. [CrossRef]
34. Pons, J.-F.; Dehaese, N.; Bourdel, S.; Gaubert, J.; Paille, B. RF power gating: A low-power technique for adaptive radios. *IEEE Trans. Very Large Scale Integr. (VLSI) Syst.* **2016**, *24*, 1377–1390. [CrossRef]
35. Bourdel, S.; Amor, I.B.; Pons, J.F.; Dehaese, N.; Vauché, R.; Gaubert, J. RF power gating techniques for ultra low power communication. In Proceedings of the 2014 10th Conference on Ph.D. Research in Microelectronics and Electronics (PRIME), Grenoble, France, 30 June–3 July 2014. [CrossRef]
36. Sun, Y.; Liu, Z.; Fu, J.; Li, X.; Shi, Y. Investigation of total dose effects in SiGe HBTs under different exposure conditions. *Radiat. Phys. Chem.* **2018**, *151*, 84–89. [CrossRef]
37. Habeenzu, B. Effect of electron radiation on small-signal parameters of NMOS devices at mm-wave frequencies. *Microelectron. Reliab.* **2020**, *107*, 113598. Available online: http://www.sciencedirect.com/science/article/pii/S0026271419306699 (accessed on 1 February 2024). [CrossRef]
38. Prakash, A.P.G.; Pradeep, T.M.; Hegde, V.N.; Pushpa, N.; Bajpai, P.K.; Patel, S.P.; Trivedi, T.; Bhushan, K.G. Comparison of effect of 5 MeV proton and Co-60 gamma irradiation on silicon NPN RF power transistors and N–channel depletion MOSFETs. *Radiat. Eff. Defect Solid* **2017**, *172*, 952–963. [CrossRef]
39. Alvin, J.; Ananth, S.; Shrinivas, P.; Mike, Z.; Vibhor, J.; Chaojiang, L.; James, A. High-resistivity SiGe BiCMOS for switch+LNA integration for WiFi front-end IC applications. In Proceedings of the 2016 13th IEEE International Conference on Solid-State and Integrated Circuit Technology (ICSICT), Hangzhou, China, 25–28 October 2016. [CrossRef]
40. Sun, Y.; Liu, Z.; Fu, J.; Shi, Y.; Li, X. Degradation and annealing characteristics of NPN SiGe HBT exposed to heavy ions irradiation. *Radiat. Phys. Chem.* **2019**, *165*, 108433. [CrossRef]
41. Sasso, G.; Rinaldi, N.; Fischer, G.G.; Heinemann, B. Degradation and recovery of high-speed SiGe HBTs under very high reverse EB stress conditions. In Proceedings of the 2014 IEEE Bipolar/BiCMOS Circuits and Technology Meeting (BCTM), Coronado, CA, USA, 28 September–1 October 2014. [CrossRef]
42. Li, P.; He, C.; Guo, H.; Guo, Q.; Zhang, J.; Liu, M. An investigation of ELDRS in different SiGe processes. *IEEE Trans. Nucl. Sci.* **2017**, *64*, 1137–1141. [CrossRef]
43. Li, Z.; Liu, S.; Song, C.; Han, N.; Adekoya, M.A. Experimental investigation of the effects of reactor neutron-gamma pulse irradiation on SiGe HBTs under different bias conditions. *IEEE Access* **2021**, *9*, 159105–159112. [CrossRef]